Eur Biophys J (2009) 38:687–700
DOI 10.1007/s00249-009-0427-z

ORIGINAL PAPER

Protein dynamics of a β-sheet protein

Marius Schmidt · Klaus Achterhold · Valeriy Prusakov · Fritz G. Parak

Received: 6 May 2008 / Revised: 12 February 2009 / Accepted: 16 February 2009 / Published online: 7 March 2009

Abstract *Rhodnius prolixus* Nitrophorin 4 (abbreviated NP4) is an almost pure β-sheet heme protein. Its dynamics is investigated by X-ray structure determination at eight different temperatures from 122 to 304 K and by means of Mössbauer spectroscopy. A comparison of this β-sheet protein with the pure α-helical protein myoglobin (abbreviated Mbmet) is performed. The mean square displacement derived from the Mössbauer spectra increases linearly with temperature below a characteristic temperature T_c. It is about 10 K larger than that of myoglobin. Above T_c the mean square displacements increase dramatically. The Mössbauer spectra are analyzed by a two state model. The increased mean square displacements are caused by very slow motions occurring on a time scale faster than 140 ns. With respect to these motions NP4 shows the same protein specific modes as Mbmet. There is, however, a difference in the fast vibration regime. The B values found in the X-ray structures vary linearly over the entire temperature range. The mean square displacements in NP4 increase with slopes which are 60% larger than those observed for Mbmet. This indicates that nitrophorin has a larger structural distribution which makes it more flexible than myoglobin.

M. Schmidt · K. Achterhold · V. Prusakov · F. G. Parak (✉)
Physics Department E17, Technical University Munich,
85747 Garching, Germany
e-mail: fritz.parak@ph.tum.de

M. Schmidt
University of Wisconsin-Milwaukee,
Milwaukee, WI 53211, USA

V. Prusakov
Institute of Chemical Physics,
RAS, 117334 Moscow, Russia

Keywords Protein dynamics · Brownian motions · Mössbauer spectroscopy · X-ray structure analysis · Nitrophorin 4

Introduction

Proteins catalyse the reactions necessary for life. For this purpose not only a stable protein structure is required. In addition concerted structural fluctuations are needed for their function. To understand how these nano-machines work, both their structures and their dynamics must be investigated. Particularly well suited for these investigations are heme proteins since they contain an internal sensor, a protoporphyrin IX coordinated by an iron, which can be probed with a large number of biophysical methods. Heme proteins perform a variety of functions, such as storage and transport of small molecules, catalysis and electron transfer. Usually, the heme is surrounded by a network of α-helical structural segments which maintain the structure and control the dynamics necessary for function. This is the reason that up to now investigations on heme protein dynamics were nearly exclusively performed using α-helical proteins. A unique exception is the nitrophorin family of heme proteins which are almost pure β-sheet proteins. They open the door to investigate the dynamics of β-sheet proteins and compare them with α-helical heme proteins.

Seven nitrophorins were identified in the saliva gland of the blood-feeding "kissing bug", *Rhodnius prolixus* (NP1-7) (Andersen et al. 1997, 1998, 2000, 2004; Andersen and Montfort 2000; Champagne et al. 1995; Ding et al. 1999; Kondrashov et al. 2004; Maes et al. 2004; Nienhaus et al. 2004; Ribeiro et al. 1993; Roberts et al. 2001; Walker 2005; Walker and Montfort 2000; Weichsel et al. 1998).

All NPs are composed of a single polypeptide chain and have a molecular mass of about 20 kDa. They store nitric oxide (NO) in the saliva gland of the insects, and transport and release NO into the tissue of a victim. NPs exist in vivo in the ferric state and bind NO in a pH-dependent way. NO is more tightly bound at the low pH (~5) predominant in the saliva gland. In the victim's tissue the pH is 7.5. NO dissociates and diffuses through the nearby capillaries to cause vasodilatation and inhibition of blood coagulation to facilitate the bug's feast on blood. At the same time, the ferric heme of NPs binds histamine released by the victim in response to the tissue damage. Histamine causes itching and initiates immune reactions. Hence, the victim's responses, which would potentially lead to the detection of the bug, are effectively suppressed.

Crystal structures have been determined for three of the nitrophorins, NP1, NP2, and NP4 (Andersen and Montfort 2000; Andersen et al. 1998; Kondrashov et al. 2004; Maes et al. 2004; Nienhaus et al. 2004; Roberts et al. 2001; Weichsel et al. 1998). Figure 1 shows a structural overview. The nitrophorins consist of an eight-stranded antiparallel β-barrel (the β-strands are labelled A–H in Fig. 1) and three short α-helical regions, labelled 1–3 in Fig. 1, adjoining the β-barrel. A highly nonplanar, ruffled heme b is inserted into the open end of the barrel. It is bound to the protein through a histidine residue (His59) on strand C. The NPs provide a large pocket distal to the heme for ligand binding. Unlike in most globins, the heme pocket does not contain a distal histidine.

Rhodnius prolixus nitrophorin 4 (called NP4 in the following), has been particularly well characterized. It consists of 185 amino acid residues. X-ray structures for

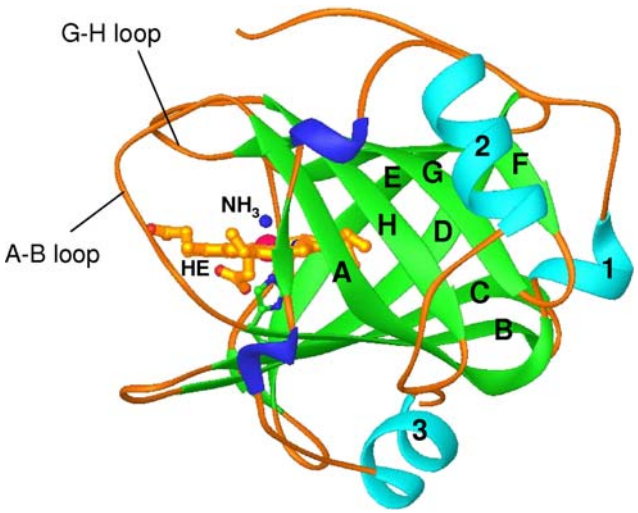

Fig. 1 The overall structure of NP4. The β-strands and α-helices are marked *A–H* and *1–3*, respectively. The position of the heme group (*HE*) in the structure and the ammonia coordinating the heme iron are also shown. Figure prepared with "ribbons" (Carson 1997)

wild type NP4 and some of its mutants, with various ligands were determined at low (~5.6) and neutral (7.0–7.5) pH at 100 K to ultrahigh resolution, up to 0.85 Å (Kondrashov et al. 2004). Of particular interest is the conformational change upon NO binding at low pH. The change is focused on the A–B loop (residues 32–40) and the G–H loop (residues 125–131) flanking the heme pocket (see also Fig. 1). In the case of NH_3 or H_2O as a ligand, NP4 has an "open" conformation where the G–H loop is located away from the heme and the heme pocket, and the A–B loop is poorly ordered. The "closed" conformation is induced for example by NO binding. This causes a collapse of the A–B and G–H loops toward the distal pockets, and hydrophobic residues pack around the ligand. The A–B loop is well ordered, and the G–H loop adopts two well-defined configurations. Both the "open" and "closed" conformers exist under all conditions with various ligands and pH values. Recently molecular dynamics simulations at pH 5 and pH 7 have been performed by selective deprotonation of the Asp 30 and Asp 35 resulting in a shift in the ratio of both conformers (Kondrashov and Montfort 2007). A highly occupied conformation under one set of conditions becomes minor one under other conditions. Therefore, these loops belong to the high-dynamic parts of the protein. FTIR spectroscopy also indicates a structural heterogeneity of NO- and CO-ligated NP4 that increases with increasing pH (Nienhaus et al. 2004). The loop heterogeneity appearing in the ultrahigh resolution structures of NP4 is consistent with its multiphasic kinetics for NO release (Maes et al. 2005).

Numerous studies on other proteins show that a functioning protein can usually adopt a number of conformations and each equilibrium conformation consists of a large number of X-ray conformational substates which have similar overall structures, but differ slightly in structural details (Frauenfelder et al. 1988). These differences can be measured by a $\langle x^2 \rangle^X$-value obtained from the crystallographic Debye–Waller factor. At physiological temperatures the proteins fluctuate between their substates. The structural fluctuations can be probed by the dynamic mean square displacement, $\langle x^2 \rangle$, of the atoms in the macromolecule [see (Parak 2003) for an overview].

The dynamics of iron containing proteins can be investigated by Mössbauer absorption spectroscopy on a time scale shorter than 140 ns using the heme iron as a probe. In the α-helical myoglobin, Mössbauer studies revealed a dramatic increase in the slope of the temperature dependence of the mean square displacements, $\langle x^2 \rangle^\gamma$, at the iron position starting at 180–200 K (Frauenfelder et al. 1988; Huenges et al. 2002; Knapp et al. 1982; Parak and Formanek 1971; Parak et al. 1982; Parak 2003). With incoherent neutron scattering this increase can also be observed for the mean square displacements, $\langle x^2 \rangle^n$,

averaged over all hydrogen atoms in the myoglobin (Doster et al. 1989; Doster and Settles 1998). The increase of the mean square displacements above about 200 K indicates an activation of protein specific motions. This so-called dynamic transition indicated by a characteristic temperature T_c has revealed itself also in many other experiments. For instance it was shown with optical absorption spectrocopy, that the electron transfer in the photosynthetic reation center of *Rhodospirillum rubrum* starts at T_c (Garbers et al. 1998; Parak et al. 1980). Optical absorption and IR spectrocopy of the nonexponential rebinding of CO after photodissociation in myoglobin showed among other features the migration of the ligand through the protein matrix above T_c (Ansari et al. 1987; Steinbach et al. 1991). IR spectrocopy also reveals a remarkable increase of a bending motion of bound NO in NP4 above T_c (Nienhaus et al. 2004). Relaxation experiments had been done with optical and with Mössbauer spectroscopy, revealing the importance of T_c for the relaxation of an intermediate state (Engler et al. 2000, 2003; Lamb et al. 1998; Prusakov et al. 1995). With X-ray structure determination it was possible to show the loss of function of ribonuclease below T_c (Rasmussen et al. 1992) and the structural changes above T_c attended with and necessary for the rebinding of CO in the L29 W mutant of myoglobin (Ostermann et al. 2000). With time-resolved transient hole-burning spectroscopy it was detected, that the time scale of myoglobin structural fluctuations and solvent dynamics are separated at room temperature and become the same at T_c (Shibata et al. 1998).

While a large number of the mentioned investigations have been performed on the purely α-helical myoglobin, the nitrophorin is an ideal object to investigate a β-sheet heme protein. In the following we employ Mössbauer absorption spectroscopy and X-ray crystallography to get a deeper insight into the static and dynamic properties of NP4 and we compare them with results obtained on myoglobin.

Materials and methods

Samples

cDNA of the NP4 was artificially synthesized (GENART, Regensburg) using the gene bank (Benson et al. 2006) sequence RPU70584 and the protein data bank (pdb) (Berman et al. 2000) entry 1D2U (Roberts et al. 2001) as a template. Codons 2–21 in the published DNA-sequence were omitted since the corresponding amino acids belong to a hydrophobic (leader) sequence which would prevent crystallization. The sequence was modified for optimal expression in *E. coli*. The construct consists of 568 base pairs including the coding sequence and NdeI and HindIII restriction sites for directional cloning. The modified cDNA was cloned into the expression vector pET17b in *E.coli* (BL21-DE3). Expression was induced with IPTG at 0.4 OD_{600} and the temperature decreased to 30°C. After shaking overnight the bacteria were harvested and the protein was found in inclusion bodies. The protein was renatured as described (Andersen et al. 1997, 1998). The protein was first solubilized in 30 mM Tris/HCl buffer (pH 7.4) containing 6 M guanidine hydrochloride, 5 mM dithiothreitol (DTT), and 1 mM EDTA and then diluted in an excess of 30 mM Tris/HCl buffer (pH 7.4) containing 0.8 mM NaCl, 1 mM EDTA, 10 mM DTT, and 15 μM phenylmethylsulphonylfluoride (PMSF) with vigorous stirring. The refolded protein was concentrated and subsequently dialysed two times against 100 mM NaP_i, pH 7.0. For the Mössbauer samples, a solution of 10 mM hemin in DMSO enriched with ^{57}Fe was added drop-wise with stirring to the refolded protein, and a possible precipitate was spun out. The formation of NP4 was monitored with UV-visible spectroscopy. The steps were repeated until the ratio of the absorption of the Soret band at 404 nm to the protein band at 280 nm remained constant. The obtained NP4 was purified by cation-exchange chromatography using a SP-Sepharose column with a gradient of 0–1.0 M NaCl.

NP4 was crystallized in 50 mM sodium phosphate, 3 M ammonium phosphate (pH 7.5), and washed two times with 3.3 M ammonium phosphate (pH 7.5). Since the NP4 crystals were grown in ammonium phosphate solution, NH_3 is bound to the heme iron at the distal position (NP4–NH_3). To prepare NP4-met(aquo) crystals NH_3 was removed from the iron-binding site by soaking the crystals repeatedly in ice-cold 3.5 M potassium phosphate (pH 7.0). The crystals of a NP4 complex which mimics the natural substrate histamine were produced by soaking the NP4–NH_3 crystals in 3.5 M potassium phosphate (pH 7.0) containing 200 mM nicotinamide adenosine dinucleotide (NADH) for 2 days on ice.

The two state model

Here we want to introduce a physical picture which was developed in order to understand the dynamics of myoglobin (Huenges et al. 2002; Knapp et al. 1982; Parak 2003). In this contribution we analyze the dynamics of NP4 with the same model in order to get a fair comparison. The two state model assumes that a protein molecule can be in two states, a frozen one and a flexible one. In the frozen state the molecules behave like any other solid. The dynamics is determined by phonons. There are no structural fluctuations. Protein specific structural fluctuations occur only in the flexible state. The number of molecules in

the frozen state and in the flexible state depends on temperature. It is determined by the probability to be in the flexible state:

$$p_{\text{flex}}(T) = (1 + e^{\frac{\Delta H_{\text{flex}} - T \cdot \Delta S_{\text{flex}}}{RT}})^{-1} \quad (1)$$

ΔH_{flex} and ΔS_{flex} are the enthalpy and the entropy difference between the frozen state and the flexible state respectively (Knapp et al. 1982). R is the general gas constant and T the temperature. In order to avoid confusion, it should be emphasized that the introduced two states do not describe two different conformations but two different flexibilities. It is well known that a protein molecule can have multiple conformations which can be recognized in ultra high resolution X-ray structure analysis. A good example is NP4 (Kondrashov et al. 2004). This variety of conformations is certainly present in the frozen state as well as in the flexible state. For our model it is, however, only important, if a molecule is frozen in an individual structure or if it can fluctuate between slightly different structures called conformational substates. The frozen as well as the flexible state represent an average over the multiple conformations, differentiating only between rigid molecules and flexible molecules.

Many physicists like Hans Frauenfelder (Frauenfelder et al. 1988) use the concept of conformational substates, CS. The word conformation is restricted to larger structural changes often connected with different functions. For example deoxymyoglobin is in the so-called *t* conformation while CO-ligated myoglobin is in the so-called *r* conformation. Molecules within one conformation (e.g. *t*), but with a slightly different structure are said to be in different CS. This concept is used for all displacements from the average structure determined by X-ray crystallography. The parameter which takes into account CS is the mean square displacement, $\langle x^2 \rangle^{\text{X}}$, where the upper index X refers to X-ray crystallography. For the two state model the $\langle x^2 \rangle^{\text{X}}$-values at the iron position are of special interest. X-ray crystallography has no time resolution. Static displacements and thermal motions can only be separated by the temperature dependence of $\langle x^2 \rangle^{\text{X}}$. In our model a molecule is either frozen in a CS or it is in the flexible state where it fluctuates till it is trapped again in a CS.

Mössbauer spectroscopy on ^{57}Fe proved to be a good tool to investigate dynamic mean square displacements, $\langle x^2 \rangle^{\gamma}$, where the upper index γ refers to γ-radiation. It should be returned to mind that energy resolution ΔE and time resolution Δt are connected by $\Delta t = \Delta E/\hbar$. Due to the high energy resolution $\Delta E = 4.7\ 10^{-9}$ eV of the ^{57}Fe Mössbauer spectroscopy, the time border becomes about 140 ns. This means that only motions on the time scale faster 140 ns contribute to $\langle x^2 \rangle^{\gamma}$. We have two contributions to $\langle x^2 \rangle^{\gamma}$:

$$\langle x^2 \rangle^{\gamma} = \langle x_{\text{v}}^2 \rangle + \langle x_{\text{flex}}^2 \rangle \quad (2)$$

The lower index "v" refers to vibrations in a CS while "flex" refers to dynamic displacements by motions in the flexible state. The vibrations in the rigid state are assumed to be harmonic and at low temperatures $\langle x^2 \rangle^{\gamma} = \langle x_{\text{v}}^2 \rangle$ [compare (Achterhold et al. 2002)]. Above a characteristic temperature T_c the flexible state is measurably populated according Eq. 1. The characteristic temperature T_{c} is not well-defined in literature. In the following we use for T_{c} the intersect of the tangent at the turning point of $\langle x_{\text{flex}}^2 \rangle$ with the temperature axis.

In the flexible state the protein or segments of the protein perform Brownian oscillations yielding the additional mean square displacement, $\langle x_{\text{flex}}^2 \rangle$. The restoring force of the Brownian oscillator is modelled by only one frequency. For the verification of the two state model the different behaviour of $\langle x^2 \rangle^{\text{X}}$ and $\langle x^2 \rangle^{\gamma}$ is essential. However, Mössbauer spectroscopy gives even more information. Broad lines in addition to the usual Lorentzians reveal diffusive motions in a limited space.

X-ray structure analysis

For the temperature dependent measurements three different crystals have been used. All low temperature experiments up to 212 K were performed on one and the same crystal. This crystal was shock frozen in a gaseous nitrogen cryostream using the crystallization buffer with 200 mg/ml of sucrose as a cryoprotectant. The temperature of the cryostream was determined at the position of the crystal using a pin-diode of size $\sim$2 mm which was calibrated by dipping it into liquid nitrogen (77 K) and ice-water (273 K). The same freezing protocol was used for the NADH and potassium phosphate soaked NP4. For measurements at ambient temperatures the crystals were mounted in capillaries. Diffraction data were collected on an Enraf-Nonius FR591 rotating anode equipped with a Siemens HiStar detector. The data were reduced using the program 'saint' (SIEMENS, Karlsruhe) and the ccp4-programs scala and truncate (CCP4 1994). The atomic model with pdb-ID 1D2U (Roberts et al. 2001) was used as a start for the refinement in CNS (Brünger et al. 1998). For all temperatures the same refinement protocol was used which comprised of a simulated annealing protocol starting from a moderate temperature (1,100 K) followed by conventional refinement of positions and B factors and a subsequent water search. The last step was a final conventional refinement of the parameters of all atoms (see Table 1). To obtain comparable values for myoglobin, the X-ray data in (Chong et al. 2001) were re-refined using the same protocol as employed for the NP4.

Table 1 Statistics from the X-ray structure determination

	Temperature									
	122 K	131 K	155 K	155 K	179 K	196 K	212 K	225 K	293 K	304 K
a	70.49	70.14	69.82	70.11	69.96	70.66	70.24	69.68	70.67	70.90
b in (Å)	42.72	42.87	42.69	42.82	42.62	42.97	42.89	42.85	43.71	43.86
c	53.06	52.88	52.66	52.82	52.68	53.01	52.93	52.56	53.19	53.40
γ	93.90	93.93	93.91	93.87	93.91	93.68	93.86	93.43	94.65	94.56
Vol (Å^3)	159,411	158,613	156,593	158,209	156,710	160,620	159,094	156651	160,683	165,530
Resol (Å)	1.5	1.5	1.5	1.5	1.5	1.5	1.5	1.75	1.5	1.5
R_{sym} (%)	3.8 (25.2)	4.3 (12.5)	4.0 (11.5)	4.1 (13.5)	4.0 (11.8)	4.2 (14.1)	3.7 (12.2)	5.9 (15.8)	5.4 (31.2)	4.3 (20.1)
Completeness (%)	92.6 (80.0)	90.0 (70.6)	89.4 (73.4)	89.2 (73.2)	90.0 (74.0)	89.0 (71.2)	89.4 (73.4)	93.8 (85.0)	91.2 (76.0)	95.2 (78.2)
Redundancy	4.6	5.0	5.0	5.0	5.0	5.0	5.0	5.6	4.6	4.6
I/σ(I)	17.0 (4.4)	12.7 (5.9)	13.9 (6.4)	13.9 (5.5)	14.1 (6.2)	13.6 (5.2)	14.7 (5.8)	10.3 (4.7)	12.2 (3.1)	12.1 (3.6)
R_{cryst}/R_{free}	19.4/22.6	19.4/22.1	19.3/21.8	19.5/22.0	19.4/22.0	19.7/22.5	19.9/21.9	20.4/21.6	19.0/21.3	19.6/22.2
N_{H_2O}	228	246	220	220	201	185	184	99	163	95
$\langle x^2\rangle^X_W$	0.126	0.150	0.153	0.151	0.151 ± 0.006	0.157	0.167	0.207 ± 0.051	0.173	0.186
$\langle x^2\rangle^X_T$	0.192	0.171	0.173	0.178	0.175	0.181	0.203	0.263	0.241	0.272
$\langle x^2\rangle^X_{NCCO}$	0.175	0.154	0.156	0.161	0.158	0.163	0.186	0.248	0.220	0.252
$\langle x^2\rangle^X_{SC}$	0.209	0.188	0.190	0.196	0.192	0.198	0.220	0.277	0.265	0.293
$\langle x^2\rangle^X_H$	0.164	0.137	0.138	0.139	0.140	0.144	0.158	0.187	0.191	0.211
$\langle x^2\rangle^X_{Fe}$	0.126	0.106	0.118	0.124	0.121 ± 0.001	0.123	0.137	0.166 ± 0.001	0.157	0.176

a, b, c and γ are the unit cell constants. *Vol* is the volume of the unit cell, *Resol* is the resolution and N_{H_2O} is the number of visible water molecules in the structure. The refinement factors R_{sym}, R_{cryst} and R_{free} have the common definition (Drenth 1998). For R_{sym}, completeness and I/σ(I) the results for the last resolution shell (1.6–1.5 Å) is given in parenthesis. Mean square displacements $\langle x^2\rangle^X$ in Å^2 are given for $\langle x^2\rangle^X_W$: from Wilson plot

$\langle x^2\rangle^X_T$: from refinement, averaged over total number of atoms

$\langle x^2\rangle^X_{NCCO}$: from refinement, averaged over backbone atoms

$\langle x^2\rangle^X_{SC}$: from refinement, averaged over side chain atoms, $\langle x^2\rangle^X_H$: from refinement, all heme atoms averaged

$\langle x^2\rangle^X_{Fe}$: from refinement, iron. Underlined temperature point: 2nd data set for 155 K after collecting seven data sets at 122, 131, 155, 179, 196 and 212 K

Mössbauer studies

For the Mössbauer experiments a large number of small NP4–NH_3 crystals ($\sim$25 mg) were sealed in a PVC holder (an inner diameter of 3 mm and 4 mm thick) with mylar windows. A ^{57}CoRh source and a conventional electromagnetic drive system with a sinusoidal velocity profile were used to measure Mössbauer absorption spectra in a temperature interval from 80 to 280 K. The temperature of the samples was adjusted with an error better than ±1 K. Typical times to measure a spectrum range from 3 days at 80 K to about 1 month at 280 K. The mean square displacement of the iron, $\langle x^2\rangle^\gamma$, is determined by the Lamb–Mössbauer factor:

$$f = \exp(-k^2\langle x^2\rangle^\gamma) \tag{3}$$

with $k = 2\pi/\lambda$, and $\lambda = 0.86$ Å for ^{57}Fe. The f-factor is proportional to the absorption area of the Mössbauer spectrum. The temperature dependence of $\langle x^2\rangle^\gamma$ obtained from the data below a characteristic temperature T_c extrapolates to zero at 0 K in the classical limit with the slope c_v. This is used to obtain an absolute calibration.

To include into the analysis also the measurements above T_c the two state model is employed, which was introduced in a preceding chapter. With this physical model the Mössbauer spectra were analyzed using the absorption cross section, σ_a, which is:

$$\sigma_a(E_a,E) = \sigma_0 \frac{\Gamma_{nat}}{2} e^{-k^2\langle x^2_v\rangle} e^{-k^2\langle x^2_{flex}\rangle} \times \sum_{N=0}^{\infty} \frac{\left[k^2\langle x^2_{flex}\rangle\right]^N}{N!} \frac{(\Gamma_a/2 + N\alpha_{flex})}{(E-E_a)^2 + (\Gamma_a/2 + N\alpha_{flex})^2} \tag{4}$$

E_a is the energy where maximal absorption occurs. The width of the Lorentzian shaped absorption is Γ_a which may be larger than Γ_{nat} determined by the life time of the Mössbauer level of ^{57}Fe. It is

$$\Gamma_a = \Gamma_{nat} + \Gamma_{inhom} + \Gamma_{relaxat} + k^2 D \tag{5}$$

Γ_{inhom} accounts for inhomogeneities of the iron environment for molecules in different CS, $\Gamma_{relaxat}$ for unresolved magnetic relaxations and k^2D for free diffusion.

While $\Gamma_{relaxat}$ decreases with temperature, k^2D increases. A separation of the different contributions is not possible in our case. σ_0 equals 2.56 10^{-18} cm^2 for ^{57}Fe. Equation 4 contains the parameters $\langle x_v^2\rangle$, $\langle x_{flex}^2\rangle$, Γ_a and α_{flex} which need to be determined. In order to get physically trustable results not all parameters are freely varied. For the evaluation we included boundary conditions and correlations. Γ_a, which is the line width of the narrow line with $N = 0$, was allowed to vary freely. As already mentioned $\langle x_v^2\rangle$ is obtained from the data below T_c. With N equal zero in Eq. 4, $\langle x_v^2\rangle$ approaches zero for $T = 0$ K. $\langle x_v^2\rangle$-values above T_c can be obtained by extrapolation using the slope c_v. Slow overdamped Brownian oscillations of larger segments within the protein molecule cause $\langle x_{flex}^2\rangle$. These motions are often called protein specific motions. α_{flex} is a parameter describing the line width of the broad lines obtained from the Brownian oscillator model. The parameters $\langle x_{flex}^2\rangle$ and α_{flex} are correlated. We have:

$$\langle x_{flex}^2\rangle = \langle x_{flex0}^2\rangle \cdot p_{flex}(T) = c_{flex} \cdot T \cdot p_{flex}(T) \quad (6)$$

and

$$\alpha_{flex} = \alpha_{flex0} \cdot p_{flex}(T) \quad (7)$$

$p_{flex}(T)$ is the probability to be in the flexible state given by Eq. 1. α_{flex0} is a constant and $\langle x_{flex0}^2\rangle$ describes the mean square displacement at the iron position due to the Brownian motions if the system would be permanently in the flexible state. $\langle x_{flex0}^2\rangle$ increases linearly with temperature with the slope c_{flex}, if we assume a simple harmonic potential for the flexible state. Inserting Eq. 6 in Eq. 7 we obtain:

$$\alpha_{flex} = \frac{\alpha_{flex0}}{c_{flex} \cdot T} \cdot \langle x_{flex}^2\rangle = \frac{c'}{T}\langle x_{flex}^2\rangle \quad (8)$$

which can be inserted into Eq. 4. While c' is a constant for all temperatures, the spectra now depend on $\langle x_{flex}^2\rangle$. All Mössbauer spectra at $T > T_c$ were fitted with an assumed c' hold constant at all temperatures. All fits were inspected. Then, c' was incremented by a small value and the procedure repeated. The best c' is determined, if satisfactory fits of the Mössbauer spectra can be observed at all temperatures. With this value of c', the $\langle x_{flex}^2\rangle$-values and, related to them by Eq. 8, the α_{flex}-values are obtained. What remains unknown at the present stage is $p_{flex}(T)$ and c_{flex}. To determine the constant c_{flex}, we assumed that the molecules populate the flexible state according to Eq.1:

Equation 1 was inserted into Eq. 6:

$$\langle x_{flex}^2\rangle = c_{flex} \cdot T/[1 + \exp((\Delta H - T\Delta S)/R/T)] \quad (9)$$

Equation 9 was fitted to the $\langle x_{flex}^2\rangle$-values weighted by $1/\sigma^2$ where σ is the standard deviation derived from the fitting of the Mössbauer spectra. From this fit, the enthalpy and entropy differences as well as the constant c_{flex} were obtained. α_{flex0} can be calculated according to Eq. 8

$$\alpha_{flext0} = c' \cdot c_{flex} \quad (10)$$

The parameter $1/\alpha_{flex0}$ is the relaxation time of the Brownian oscillator. With $\Delta x(t) = x_{flex}(t) - x_{flex}(0)$ one obtains

$$1/2\left\langle \Delta x(t)^2 \right\rangle = \langle x_{flex}^2\rangle \cdot (1 - \exp(-\alpha_{flex0} \cdot t)) \quad (11)$$

An iron at the position $x_{flex}(0)$ at the time zero is at position $x_{flex}(t)$ at time t. α_{flex0}^{-1} measures the time which it takes that ½ $\Delta x(t)^2$ approximates $\langle x_{flex}^2\rangle$ (Knapp et al. 1982).

The temperature dependence of the total $\langle x^2\rangle^\gamma$ in the entire temperature range is finally given by Eq. 12, which connects the vibrational part c_v with the quasi diffusive part c_{flex} and the probability of the molecules to be in the flexible state:

$$\langle x^2\rangle^\gamma = \langle x_v^2\rangle + \langle x_{flex}^2\rangle = c_v \cdot T + c_{flex} \cdot T \cdot p_{flex}(T) \quad (12)$$

In order to improve the myoglobin data with respect to the literature we measured the Mössbauer spectra of Mbmet crystals and applied the same analysis procedure as in the case of NP4.

Results and discussion

X-ray structure analysis

The statistics of the temperature dependent X-ray structure determination and those of the NP4met(aquo) and the NP4 complex with nicotinamide are given in Tables 1 and 2, respectively. The space group of all crystals is C2. The overall structure of NP4–NH_3 determined with 1.5 Å resolution (Figs. 1, 2a) is in good accordance with the open conformation structure of NP4–NH_3 obtained earlier (Andersen et al. 1998; Kondrashov et al. 2004; Roberts et al. 2001). The heme is found in a double position. The two heme positions differ by a 180° rotation about the CHA–CHC axis, which has been modelled by a conformer ratio of 1:1. Other authors report conformer ratios of ~3:2 (Roberts et al. 2001). With ammonium phosphate as crystallization buffer, ammonia is bound to the iron with an iron to nitrogen distance of ~2.1 Å at all temperatures. Four additional water molecules can be found in the heme pocket at $T < 200$ K (positions 2–5 in Fig. 2a, b). However, at temperatures of 225 K and higher the water structure rearranges and only two of these water positions can be identified. Obviously, there is an onset of dynamics which affects the water structure in the heme pocket above 200 K.

Table 2 Unit cells and statistics of the X-ray structure determination using NP4 crystals soaked in potassium phosphate [NP4met(aquo)] and NADH (NP4-nicotinamide) respectively

	NP4met(aquo) 140 K	NP4-nicotinamide 140 K
a	70.08	69.58
b in (Å)	42.82	42.66
c	52.45	52.29
γ	93.94	93.83
Resol (Å)	1.55	1.6
R_{sym} (%)	3.9 (14.6)	4.7 (22.6)
Compl (%)	82.4 (61.2)	90.0 (77.8)
Redund	5.8	5.8
I/σ(I)	15.0 (5.3)	13.6 (3.3)
R_{cryst}/R_{free}	19.6/23.4	20.1/23.0
N_{H_2O}	269	152

All abrreviations as in Table 1

When the ammonium phosphate buffer is replaced by potassium phosphate, a water molecule is found as the 6th Fe(III) ligand with an Fe–O distance of 1.85 Å (position 1). Figure 2b shows the X-ray structure for NP4met(aquo) at pH 7.0 and 120 K. Besides the water on position 1 four additional water molecules occupy the heme pocket. If NP4 crystals are incubated with NADH electron density appears in the heme pocket that equals that of nicotinamide (Fig. 2c). Additional electron density that might belong to the rest of NADH cannot be identified. NP4 cleaves NADH into nicotinamide and presumably adenosine diphosphate ribose and binds one of the fragments namely nicotinamide. The pyridine ring of the nicotinamide is bound via its ring nitrogen to the iron replacing the heme bound water molecule as well as the other water molecules in the heme pocket. The mechanism of the cleavage is not understood. Nevertheless, both the water structure in the heme pocket as well as the nicotinamide structure mimic that of the natural NP4 substrate which is histamine.

Besides the structure of the average conformation, X-ray data analysis yields the crystallographic *B* factor that is a measure of the mean square displacements of the atoms, $\langle x^2 \rangle^X$, from their average positions:

$$\langle x^2 \rangle^X = B/(8\pi^2), \tag{13}$$

B is the crystallographic *B* value, often called temperature factor.

To separate static and dynamic effects, X-ray structures were determined over a temperature range from 122 to 304 K. Figure 3a shows the $\langle x^2 \rangle^X$ as a function of the residue number at 131 and 304 K. One can identify regions with low $\langle x^2 \rangle^X$, which belong to the β-strands A–H, and

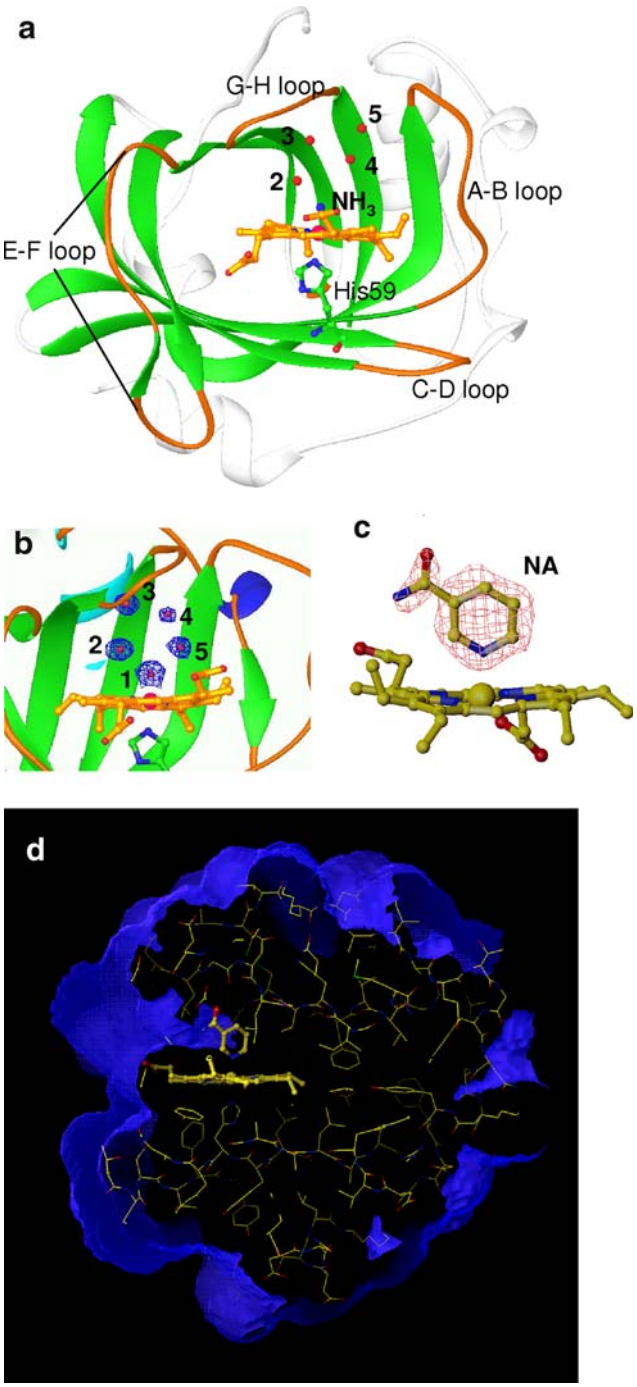

Fig. 2 Results from the X-ray structure determination. **a** View into the β-barrel. All four loops flanking the heme are shown. **b** The heme pocket of NP4, if crystals are soaked in potassium phosphate. Water molecules forming the ring like structure are marked *1–5*. Electron density (*blue*) contoured at 1σ. **c** The heme pocket of NP4 soaked with 200 mmol/L NADH. *NA* nicotinamide. Electron density (*red*) contoured at 1σ. **d** Water accessible surface (*blue*) of the NP4 (probe radius 1.4 Å) shows water channel into the heme pocket. The nicotinamide bound to the heme is shown in addition. Figure prepared with "ribbons" (Carson 1997) and "O" (Jones et al. 1991)

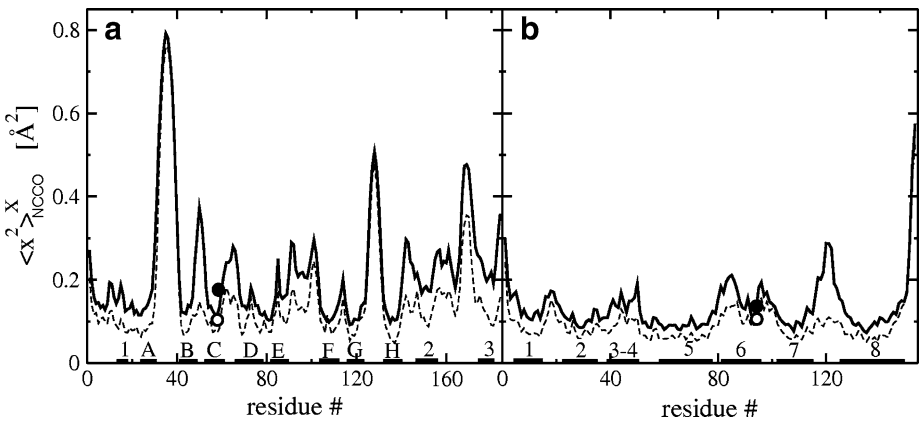

Fig. 3 The $\langle x^2 \rangle^X_{NCCO}$ averaged over the backbone atoms N, C_α, C and O plotted as a function of the residue number for nitrophorin (**a**) and myoglobin (**b**). *Solid line* room temperature, *dashed line* 131 K. *Solid* and *open spheres* $\langle x^2 \rangle^X_{Fe}$ of the heme iron at room temperature and 131 K, respectively. **a** Results for NP4, *A–H*: β-strands, *1–3*: short α-helices, **b** results for Mbmet, *1–8*: α-helical segments in myoglobin

regions with high $\langle x^2 \rangle^X$, which belong to the flexible loops. Most of the residues such as those in the B–C loop show a strong temperature dependence of their $\langle x^2 \rangle^X$ which indicates a large contribution of dynamics. With decreasing temperature the molecules occupy substates with lower energy and the structural distribution becomes more confined. However, there are also regions such as the A–B and the G–H loop, which behave quit different. They exhibit the highest *B* values which are, however, almost temperature independent. For comparison, backbone mean square displacements of myoglobin are given in Fig. 3b.

The temperature dependence of $\langle x^2 \rangle^X$ averaged over all the backbone (N, C_α, C, O) atoms ($\langle x^2 \rangle^X_{NCCO}$) of NP4 and that of the heme iron, $\langle x^2 \rangle^X_{Fe}$, is plotted in Fig. 4. The temperature dependences were fitted by straight lines with slopes c^X in analogy to myoglobin [see (Parak et al. 1987b) for a detailed discussion of this behaviour]. The

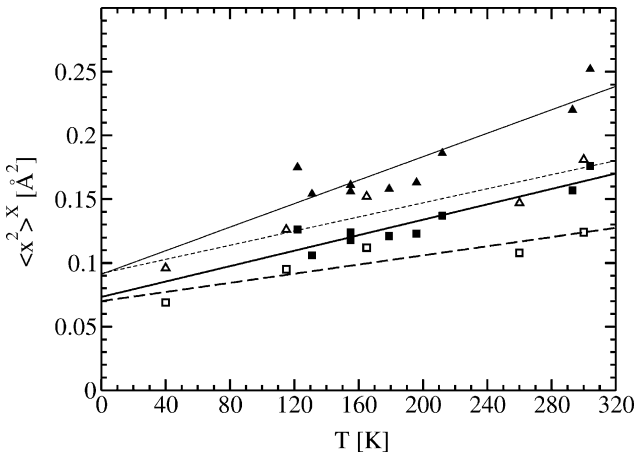

Fig. 4 Temperature dependence of the $\langle x^2 \rangle^X$ determined from the crystallographic *B* value. *Solid triangles* $\langle x^2 \rangle^X_{NCCO}$ averaged over the backbone atoms of NP4, *solid squares* $\langle x^2 \rangle^X_{Fe}$ of the NP4 heme iron, *open triangles* $\langle x^2 \rangle^X_{NCCO}$ averaged over the backbone atoms of Mbmet, *open squares* $\langle x^2 \rangle^X_{Fe}$ of the Mbmet heme iron. *Thin solid, thick solid, thin dashed* and *thick dashed lines* are linear fits to the data for NP4 backbone atoms, NP4 iron, Mbmet backbone atoms and Mbmet iron, respectively

extrapolation to $T = 0$ K gives an estimate of the static distribution of the structure. In the case of the A–B loop the average mean square displacement, $\langle x^2 \rangle^X_{AB}$, extrapolates with temperature to 0.52 Å^2 at 0 K which would mean that 80% of its total mean square displacement at 304 K ($\langle x^2 \rangle^X_{AB} = 0.65$ Å^2) is static and only 20% dynamic. This is unlikely at room temperature. The energy surface of the AB-loop seems to be very shallow. At low temperatures the AB-loop can adopt many different structures having almost the same energy and the structural distribution is indeed static. At higher temperatures the loop effectively fluctuates between these different substates exploring only few in addition.

To test a possible redistribution of conformational substates during the raise of the temperature and to check for a potential influence of radiation damage, the measurement at 155 K was performed twice on the same crystal. The first data set was measured after previous experiments at 122 and 131 K. The second data set was measured after recording data sets at 179 K, 196 K, and 212 K. The corresponding $\langle x^2 \rangle^X$ values obtained in both 155 K experiments are nearly the same. This implies that radiation damage and a possible photoreduction of Fe(III) to Fe(II) does not play a significant role in our experiments. Irreversible position and orientation changes of the NP4 molecule in the crystal during the temperature cycle can be excluded. This result shows in addition that the flash-freezing procedure does not produce an artificial metastable structural distribution. Such a structural distribution would collapse at elevated temperatures and *B* values derived from the second 155 K data set would have changed. This is not observed and the thermodynamic equilibrium between the substates is maintained at all temperatures.

Mössbauer spectra

Figure 5 shows Mössbauer spectra of the polycrystalline sample of NP4–NH_3 measured in a transverse magnetic

field of 20 mT. In the temperature range of 80–210 K the spectra can be well fitted with a single asymmetric quadrupole doublet with somewhat broadened lines (Fig. 5a–c). The values and the temperature dependence of the Mössbauer parameters which are the isomer shift, IS, the quadrupole splitting, QS, and the linewidths, Γ_a, show that the heme iron is in the Fe(III) low spin state (Table 3). The temperature dependent asymmetry of the quadrupole doublet is the signature of Fe(III). The signature for low spin is the large quadruple splitting together with the decrease of the linewidth asymmetry with increasing temperature in the temperature regime below T_c where no protein specifying motional modes were present. Such a behaviour is typical of Fe(III) low spin heme proteins, e.g. ferricytochromes (Cooke and Debrunner 1968; Debrunner 1989; Lang et al. 1968; Sharrock et al. 1973). With increasing temperature the spin-lattice relaxation time becomes faster and $\Gamma_{relaxat}$ decreases. In the fast relaxation limit both components of the doublet become equally narrow. The area ratio of the left- to the right-hand line ($A_{(l)}/A_{(r)}$) is about 0.83 in all the temperature range (see Table 3), and can be explained by joint appearance of two factors: (1) an anisotropy of the relative intensities of the absorption lines depending on an angle between the direction of the Mössbauer γ quanta and the axis of the gradient of the electric field at the heme iron in the NP4–NH_3; and (2) partial orientation of the small protein crystals of plate form in the Mössbauer sample (Gol'danskii and Makarov 1968). The increase of Γ_a above T_c is an indication of a contribution k^2D (compare Eq. 5). Our data do not allow a separation of the different contributions to Γ_a.

Figure 6 shows the temperature dependence of $\langle x^2\rangle^\gamma$ of the iron atom in the polycrystalline sample of NP4–NH_3 together with the values obtained for metmyoglobin. Two regimes can be distinguished. Below the characteristic temperature T_c the $\langle x^2\rangle^\gamma$ values increase linearly with temperature typical for solid state vibrations. As shown for myoglobin the phonon density of states (Achterhold et al. 2002; Huenges et al. 2002) or a normal mode analysis (Chong et al. 2001) can fully account for this temperature behaviour. Each protein molecule within the ensemble vibrates in a distinct conformational substate, whereas the structure of each substate differs slightly. Above T_c the slope of the $\langle x^2\rangle^\gamma$ versus T deviates from the linear increase. Protein specific motions are activated, indicated also by the appearance of the broad lines in the Mössbauer spectra and the strong decrease of the intensity of the narrow lines. The broad components in the spectra obtained above T_c are indicative for the diffusive like motions of NP4 segments in limited space. The molecules leave their substates and fluctuate with large amplitude motions in the flexible state. The temperature dependence of $\langle x^2_{flex}\rangle^\gamma$ allows the determination of the thermodynamic parameters ΔH and ΔS as

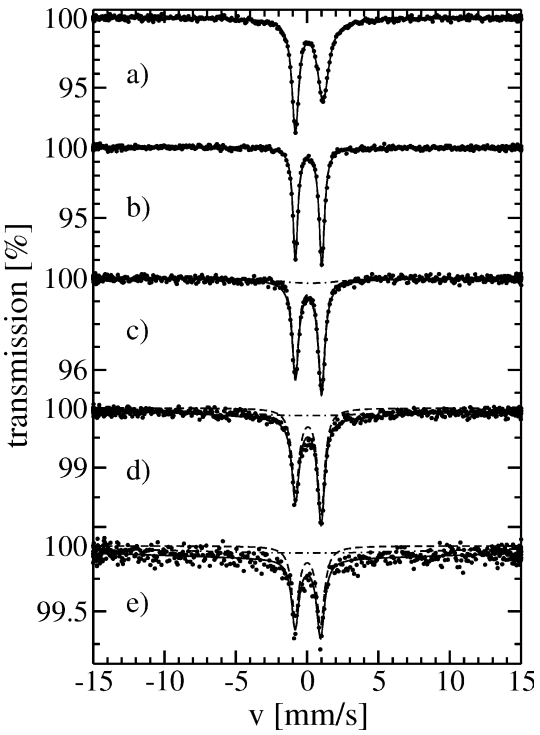

Fig. 5 Mössbauer spectra from the NP4 crystals at **a** 80 K, **b** 180 K, **c** 220 K, **d** 260 K, **e** 280 K. *Thick solid lines* least squares fit to the Mössbauer spectra using Eq. 4. Fits at 80 and 180 K could be performed with $N = 0$ only. For the higher temperatures $N = 0$ (contribution shown by *dashed lines*) and $N = 1$–20 (contributions shown by *dashed dotted lines*) of Eq. 4 were taken into account. The contributions of terms with $N > 6$ were less than 1%

well as the constant c_{flex} derived by Eq. 9 and listed in Table 4. Equation 11 allows us to calculate the relaxation time of the Brownian oscillator. At 280 K the relaxation of $1/2\left\langle \Delta x(t)^2 \right\rangle$ into 95% of the equilibrium value of $\langle x^2_{flex}\rangle^\gamma$ occurs in about 10 ns.

The different temperature dependences of X-ray and Mössbauer data

Besides the $\langle x^2\rangle^\gamma$ values obtained by Mössbauer spectroscopy for NP4 and Mbmet, Fig. 6 also shows the $\langle x^2\rangle^X_{Fe}$-values derived from the X-ray data of NP4. At all temperatures the $\langle x^2\rangle^X_{Fe}$-value at T = 0 K has been subtracted, to obtain only the temperature dependent part. It is evident that $\langle x^2\rangle^\gamma$ and $\langle x^2\rangle^X_{Fe}$ differ strongly. This discrepancy is caused by the different time sensitivity of the two experimental methods. The $\langle x^2\rangle^\gamma$-values are caused by self-correlation. Mössbauer spectroscopy is sensitive to the dynamics of individual molecules. Due to the energy resolution of about 5 neV, Mössbauer spectroscopy can measure structural fluctuations with a characteristic time faster than 140 ns. The temperature dependence of the $\langle x^2\rangle^X_{Fe}$-values can be approached by a linear increase with

Table 3 Parameter of the Mössbauer spectra of NP4–NH_3 crystals

T, K	$IS_{\alpha\text{-Fe}}$ mm/s	QS mm/s	$\Gamma_{a(l)}$ mm/s	$\Gamma_{a(r)}$ mm/s	$\Gamma_{a(l)}/\Gamma_{a(r)}$	$A_{(l)}/A_{(r)}$
80	0.258 ± 0.003	1.944 ± 0.005	0.585 ± 0.005	0.970 ± 0.009	0.604 ± 0.008	0.828 ± 0.012
120	0.238 ± 0.002	1.892 ± 0.003	0.447 ± 0.004	0.611 ± 0.005	0.733 ± 0.009	0.810 ± 0.010
140	0.231 ± 0.002	1.866 ± 0.003	0.413 ± 0.004	0.525 ± 0.005	0.786 ± 0.011	0.825 ± 0.012
180	0.214 ± 0.002	1.855 ± 0.003	0.410 ± 0.004	0.475 ± 0.004	0.863 ± 0.012	0.867 ± 0.013
220	0.207 ± 0.003	1.834 ± 0.007	0.4	0.4	1	0.83
240	0.199 ± 0.005	1.813 ± 0.011	0.4	0.4	1	0.83
260	0.193 ± 0.005	1.800 ± 0.010	0.4	0.4	1	0.83
280	0.163 ± 0.012	1.780 ± 0.024	0.4	0.4	1	0.83

$\Gamma_{a(l)}$, $\Gamma_{a(r)}$, $A_{(l)}$ and $A_{(r)}$ are the linewidths and the areas of the left and right absorption lines respectively. The ratio of the areas $A_{(l)}/A_{(r)}$ for 220, 240, 260 and 280 K was fixed for the fitting to the low temperature, 80 K, date. The linewidths Γ_a where both fixated to the extrapolated value of 0.4 mm/s for these temperatures

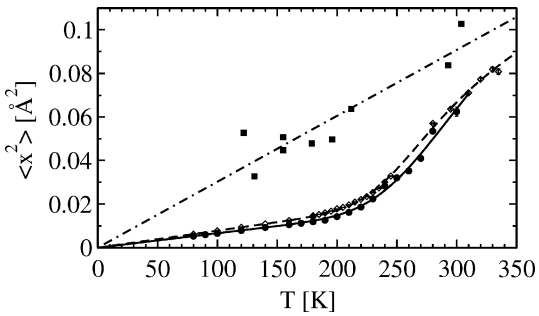

Fig. 6 The temperature dependence of the mean square displacements $\langle x^2\rangle^\gamma$ of the heme iron in NP4 and Mbmet determined from the Mössbauer spectroscopy compared to the dynamic mean square displacement $\langle x^2\rangle^X_{Fedyn}$ calculated from the crystallographic *B* value of the heme iron in NP4. *Solid spheres* $\langle x^2\rangle^\gamma$ of the NP4. *Open diamonds* $\langle x^2\rangle^\gamma$ of the Mbmet. *Error bars* are mostly smaller than symbol size. *Thick solid line* the temperature dependence of the $\langle x^2\rangle^\gamma$ as determined by Eq. 2 with Eq. 9 for NP4. *Dashed line* the temperature dependence of the $\langle x^2\rangle^\gamma$ as determined by Eq. 2 with Eq. 9 for Mbmet. *Solid squares* $\langle x^2\rangle^X_{Fedyn}$ of NP4. *Dashed dotted line* assumed linear temperature dependence of $\langle x^2\rangle^X_{Fedyn}$

Table 4 Parameters obtained from the fits to the $\langle x\rangle^\gamma$ of NP4–NH_3 and Mbmet crystals

	NP4–NH_3	Mbmet
c_v (Å^2 K^{-1})	(6.6 ± 0.2) × 10^{-5}	(7.8 ± 0.1) × 10^{-5}
c_{flex} (Å^2 K^{-1})	(2.66 ± 1.27) × 10^{-4}	(1.97 ± 0.08) × 10^{-4}
$c_v + c_{flex}$ (Å^2 K^{-1})	(3.32 ± 1.27) × 10^{-4}	(2.75 ± 0.08) × 10^{-4}
ΔH_{flex} (kJ mol^{-1})	18300 ± 3700	21000 ± 960
ΔS_{flex} (kJ mol^{-1} K^{-1})	63 ± 20	80 ± 4
α_{flex0} (mm s^{-1})	44.3 ± 21.2	32.8 ± 1.3
Slopes c^X (Å^2 K^{-1})		
c^X_{Fe}	(3.02 ± 0.49) × 10^{-4}	(1.80 ± 0.48) × 10^{-4}
c^X_{NCCO}	(4.61 ± 0.88) × 10^{-4}	(2.76 ± 0.66) × 10^{-4}

c_v is the slope of $\langle x\rangle^\gamma$ below the characteristic temperature T_c, c_{flex} is the slope within the flexible state. ΔH_{flex} and ΔS_{flex} are the enthalpy and the entropy difference between the frozen state and the flexible state respectively. α_{flex0} is the width of the broad Lorentzians in Eq. 4 if the molecules are permanently in the flexible state. For comparison the temperature dependences of the slopes c^X of the iron (c^X_{Fe}) and the backbone (c^X_{NCCO}) determined from the *B* values are given

temperature although the values scatter strongly. X-ray crystallography is sensitive to pair correlations. The $\langle x^2\rangle^X$-values are an average of structural distributions of all conformational substates throughout the crystal as well as an average over vibrations and fluctuations. There is no differentiation between static and dynamic displacements. However, since the static part of the $\langle x^2\rangle^X$ can be estimated by extrapolation to 0 K, it can be subtracted to obtain the dynamic part only. At the position of the iron we obtain $\langle x^2\rangle^X_{Fedyn}$. If the $\langle x^2\rangle^X_{Fedyn}$-value is larger than the $\langle x^2\rangle^\gamma$-value of the iron atom at the same temperature (see Fig. 6), then displacements contribute to the $\langle x^2\rangle^X_{Fedyn}$ which are caused from motions slower than 140 ns.

Assuming a linear decrease of $\langle x^2\rangle^X_{Fedyn}$ with temperature implies that the thermal equilibrium is reached fast in comparison to the time of the experiment. We may estimate this time assuming that for a relaxation into the equilibrium the flexible state has to be reached. At temperatures below T_c the Brownian motions are very ineffective. At 100 K p_{flex} is 5.4 × 10^{-7} for NP4 and not even every millionth molecule is in the flexible state. However, in the crystalline ensemble, which consists of roughly 10^{14} molecules, about 5 × 10^7 proteins are in the flexible state at the same time, each molecule for a period of time that corresponds to a few protein specific motions which are in the order of a few nano-seconds until it returns to the rigid state (Parak 2003). From this one may estimate that at 100 K a few seconds are sufficient for a distribution to equilibrate after a temperature change which is very short compared to the time needed to collect the X-ray data. Only when the temperature is decreased so much that the probability to leave the substate is so low that it is extremely unlikely that any of the molecules of the

ensemble enters the flexible state during the recording of an X-ray structure, then the distribution is frozen out. On a time scale of 10^2 s, which is about the time that is needed to collect a monochromatic data set at a synchrotron, p_{flex} should be as low as 10^{-24} assuming 10^{14} molecules in a crystal and a 10 ns residence time in the flexible state. By rewriting Eq. 9 with respect to T and with the ΔH and ΔS shown in Table 4 one can estimate the temperature at which this p_{flex} is reached. For NP4, T needs to be decreased to about 36 K. Using ΔH and ΔS for myoglobin shown in Table 4 we arrive at 39 K, which is the temperature needed to effectively capture and stabilize the CO in crystallographic photo-flash experiments on MbCO (Hartmann et al. 1996; Schlichting et al. 1994; Teng et al. 1994, 1997).

Comparison of nitrophorin and myoglobin

In the following the results on the β-sheet nitrophorin are discussed in the light of existing experiments on the α-helical myoglobin. Figures 3 and 4 compare the mean square displacements $\langle x^2\rangle^{\mathrm{X}}$ averaged over the backbone atoms of individual residues in NP4–NH_3 and Mbmet. The atomic distributions are larger for NP4 than for Mbmet. In NP4 the large, flexible loops are tethered between relatively stable β-strands (A–H) whereas in Mbmet only the loop between helix 7 and 8 shows pronounced B values. The three small helices 1–3 in NP4 show larger B values than the β-strands or the helices in Mbmet. The reason might be that they are at the periphery of the protein (see Fig. 1) and may slide on the β-barrel whereas in Mbmet the helices are integral part of the protein structure.

Following the line for myoglobin (Chong et al. 2001; Parak et al. 1987b), the temperature dependencies of the $\langle x^2\rangle^{\mathrm{X}}_{\mathrm{Fedyn}}$ for NP4 was approximated by a straight line. Linear extrapolation for NP4 gives, like for Mbmet, a positive $\langle x^2\rangle^{\mathrm{X}}_{\mathrm{Fe}}$ at $T = 0$ K that can be considered as the static part, $\langle x^2\rangle^{\mathrm{X}}_{\mathrm{Festat}}$, of the $\langle x^2\rangle^{\mathrm{X}}$ values. $\langle x^2\rangle^{\mathrm{X}}_{\mathrm{Festat}}$ is caused by molecules having slightly different structures but can not be distinguished with respect to their energy. Although the $\langle x^2\rangle^{\mathrm{X}}$ of NP4 are higher overall than those of myoglobin, the corresponding lines intersect at similar positions at $T = 0$. Obviously, the average static disorder is similar in nitrophorin and myoglobin. The double position of the entire heme group which is observed in the crystal structure of NP4 does not seem to contribute to the static disorder since the iron positions in these two heme orientations superpose perfectly.

If the temperature is increased, more substates are populated and the distributions of atomic positions in the crystal changes. The temperature dependence of $\langle x^2\rangle^{\mathrm{X}}$ is larger in NP4 than in Mbmet (Figs. 3, 4). This can be observed especially at the iron position (Fig. 4). The slope c^{X} obtained is 3×10^{-4} Å^2/K for the NP4 iron and about 2×10^{-4} Å^2/K for myoglobin for the Mbmet iron (Table 4). In NP4 the $\langle x^2\rangle^{\mathrm{X}}_{\mathrm{Fedyn}}$ changes from 0.11 to about 0.18 Å^2 when going from cryogenic temperatures to 300 K whereas in Mbmet it drops only from 0.12 at 300 K to 0.10 at 115 K. A wider set of conformational substates can be explored at a certain temperature in nitrophorin. This may make NP4 more flexible than the myoglobin. At 100 K the dynamic mean square displacement of the central iron is 0.03 Å^2 which is about 30% of the total $\langle x^2\rangle^{\mathrm{X}}_{\mathrm{Fe}}$. This is in accordance with results from another study at atomic (<1 Å) resolution (Petrova et al. 2006). At 293 K the $\langle x^2\rangle^{\mathrm{X}}_{\mathrm{Fedyn}}$ is 0.09 Å^2 for the iron, which is 57% of the total mean square displacement for NP4 (compare Figs. 6, 4), and 0.06 Å^2 for myoglobin, which is also roughly 50% of the total mean square displacement.

The characteristic temperature, T_c of NP4 is around 230 K, which is about 10 K larger than that of myoglobin. Note, that with our definition the T_c values become slightly larger as those in literature. The characteristic temperature can also be identified in FTIR investigations on the NP4–NO complex (Nienhaus et al. 2004). Large amplitude bending motions of the NO set on only at $T > 220$ K in good accordance with the T_c determined here.

Figure 7 compares the $\langle x^2_{\mathrm{flex}}\rangle$-values of NP4 and Mbmet. There are slight differences which are larger than the error bars. Table 4 shows the entropy and enthalpy differences for NP4 and Mbmet as determined by fitting Eq. 9 to the $\langle x^2_{\mathrm{flex}}\rangle$-values. However, taking the error bars in consideration, the values for the two proteins are practically the same. The differences in the $\langle x^2\rangle$-values are not large enough to give significant differences in ΔH or ΔS. The results depend on the fine interplay between the parameter c_{flex}, ΔH and ΔS which are to some extend correlated. c_{flex} is a measure of the width of the flexible state. ΔH parameterizes the depth of the rigid state. ΔS determines the entropy loss, when a molecule returns to the rigid state,

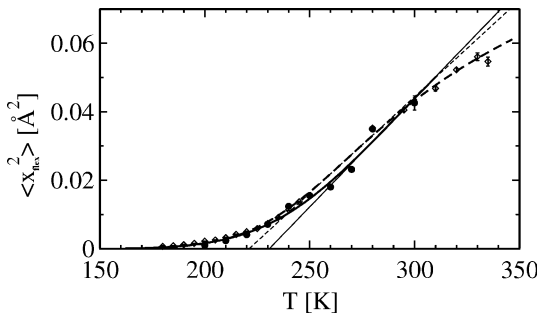

Fig. 7 Comparison of the temperature dependence of the mean square displacement in the flexible state $\langle x^2_{\mathrm{flex}}\rangle$ for NP4 (*solid spheres*) and Mbmet (*open diamonds*). *Error bars* are mostly smaller than symbol size. *Thick solid line* result of fitting Eq. 9 to the $\langle x^2_{\mathrm{flex}}\rangle$ of NP4. *Thick dashed line* result of fitting Eq. 9 to the $\langle x^2_{\mathrm{flex}}\rangle$ of Mbmet. *Thin solid line* and *thin dashed line* tangent of $\langle x^2_{\mathrm{flex}}\rangle$ at the turning point for NP4 and Mbmet respectively

Table 5 Comparison of $\langle x^2_{\text{flex}}\rangle^{\gamma}$ and α_{flex} derived from the Mössbauer investigations at $T \geq 180$ K for NP4–NH_3 and Mbmet

	Temperature					
	180 K	200 K	220 K	240 K	260 K	280 K
NP4–NH_3						
$\langle x^2_{\text{flex}}\rangle^{\gamma}$ (Å^2)	0.0	0.0010	0.0041	0.0124	0.0180	0.0350
α_{flex} (mm/s)	0.0	0.83	3.11	8.61	11.54	20.83
Mbmet						
$\langle x^2_{\text{flex}}\rangle^{\gamma}$ (Å^2)	0.0006	0.0022	0.0050	0.0113	–	0.0352
α_{flex} (mm/s)	0.56	1.83	3.79	7.85	–	20.95

and which therefore keeps the molecules in the flexible state (Table 5).

Discussion

In our investigations we were able to separate dynamics in three time regimes. Fast vibrations revealed itself by the $\langle x^2\rangle$-values of the iron in NP4 at temperatures below T_c obtained from ^{57}Fe Mössbauer spectroscopy. Above T_c Mössbauer spectroscopy reveals in addition protein specific motions on a time scale faster than 140 ns. The relevant parameters are$\langle x^2_{\text{flex}}\rangle$ and α_{flex}. Structural distributions on all time scales were obtained from X-ray structure analysis. Beside the $\langle x^2\rangle^{X}_{Fe}$-value of the heme iron also $\langle x^2\rangle^{X}_{NCCO}$-values for the backbone atoms have been determined.

There are clear differences in $\langle x^2_v\rangle$ for NP4 and Mbmet. The larger values for NP4 compared to Mbmet indicate that NP4 together with the buffer are a softer system, at least at the position of iron. It is unlikely that this is caused by the different buffer (3.3 M ammonium phosphate for NP4 and 3.6 M ammonium sulphate for Mbmet). It probably reflects the fact the the heme group in Mbmet is buried in the protein moiety, while it is more on the surface in NP4.

Above T_c quasi diffusive motions are exited which can be described by Brownian motions in limited space of molecular segments. Astonishingly, these protein specific motions are the same for NP4 and Mbmet. On a first sight it seems more likely that these motions are different in a β-sheet protein and in an α-helical protein. Since this is not the case we have to look for an explanation. It is well known that the protein specific motions are strongly coupled to the mobility of the hydration shell (Fenimore et al. 2002, 2004; Frauenfelder et al. 2006). If the protein looses its hydration shell by freeze drying it becomes rigid (Parak et al. 1987a). A correlation between the mobility of adsorbed water and protein dynamics was already found by Singh et al. (Singh et al. 1981). It is also known that the temperature dependence of dielectric relaxation for water adsorbed in Mbmet crystals is very similar to that of water adsorbed on many other materials (Hedvig 1977). That means that the fluctuation of the surface water is probably very similar in NP4 and Mbmet. Going back to our two state model we assume that the fluctuation of the water molecules determines $p_{\text{flex}}(T)$. One mechanism may be that fluctuating water molecules shield the charged residues on the protein surface much better from each other than rigid waters with a low ε. A diminished interaction of the surface charges of the protein reduces the rigidity.

Clear differences between the dynamics of NP4 and Mbmet can be obtained from X-ray structure analysis. The structural distribution is larger in NP4 than in Mbmet. This enables the nitrophorin to allow ligands like histamine and nicotinamide and most likely even NADH to enter the heme pocket easily. Without too much drag, these ligands replace the water structure there and bind to the iron. The mentioned structural heterogeneity of the A–B and G–H loops flanking the heme pocket in NP4 is in accordance with this behaviour. The β-barrel provides a flexible entrance to the heme pocket. Big channels to the heme pocket can be opened transiently for the substrate to enter. In contrast, the architecture of the myoglobin is more compact in their functional form to bind smaller ligands. Also here transient channels need to be opened to allow the ligands to enter. However, these channels do not need to be big. The small ligands like O_2 or CO can penetrate more easily and require a less flexible architecture.

Acknowledgment This research was supported by the German Research Foundation (DFG) under Grants No. PA 178/28-1 and PA 178/28-2.

References

Achterhold K, Keppler C, Ostermann A, van Bürck U, Sturhahn W, Alp EE, Parak FG (2002) Vibrational dynamics of myoglobin determined by phonon assisted Mössbauer effect. Phys Rev E 65:051916-1–051916-13

Andersen JF, Montfort WR (2000) Crystal structures of nitrophorin 2: a trifunctional antihemostatic protein from the saliva of *Rhodnius prolixus*. J Biol Chem 275:30496–30503. doi:10.1074/jbc.M002857200

Andersen JF, Champagne DE, Weichsel A, Ribeiro JMC, Balfour CA, Dress V, Montfort WR (1997) Nitric oxide binding and crystallization of recombinant nitrophorin I, a nitric oxide transport protein from the bloodsucking bug *Rhodnius prolixus*. Biochemistry 36:4423–4428. doi:10.1021/bi9628883

Andersen JF, Weichsel A, Balfour CA, Champagne DE, Montfort WR (1998) The crystal structure of nitrophorin 4 at 1.5 Å resolution: transport of nitric oxide by a lipocalin-based heme protein. Structure 6:1315–1327. doi:10.1016/S0969-2126(98)00131-2

Andersen JF, Ding XD, Balfour C, Shokhireva TK, Champagne DE, Walker FA, Montfort WR (2000) Kinetics and equilibria in ligand binding by nitrophorins 1–4: evidence for stabilization of a nitric oxide–ferriheme complex through a ligand-induced conformational trap. Biochemistry 39:10118–10131. doi:10.1021/bi000766b

Andersen JF, Gudderra NP, Francischetti IMB, Valenzuela JG, Ribeiro JMC (2004) Recognition of anionic phospholipid membranes by an antihemostatic protein from a blood-feeding insect. Biochemistry 43:6987–6994. doi:10.1021/bi049655t

Ansari A, Berendzen J, Braunstein D, Cowen BR, Frauenfelder H, Hong MK, Iben IET, Johnson JB, Ormos P, Sauke TB, Scholl R, Schulte A, Steinbach PJ, Wittitow J, Young RD (1987) Rebinding and relaxation in the myoglobin pocket. Biophys Chem 26:337–355. doi:10.1016/0301-4622(87)80034-0

Benson DA, Karsch-Mizrachi I, Lipman DJ, Ostell J, Wheeler DL (2006) GenBank. Nucleic acids Research 34 Database issue: D16–D20

Berman HM, Westbrook J, Feng Z, Gilliland G, Bhat TN, Weissig H, Shindyalov IN, Bourne PE (2000) The protein data bank. Nucleic Acids Res 28:235–242. doi:10.1093/nar/28.1.235

Brünger AT, Adams PD, Clore GM, DeLano WL, Gros P, Grosse-Kunstleve RW, Jiang J-s, Kuszewski J, Nilges M, Pannu NS, Read RJ, Rice LM, Simonson T, Warren GL (1998) Crystallography and NMR system: a new software suite for macromolecular structure determination. Acta Crystallogr D Biol Crystallogr 54:905–921. doi:10.1107/S0907444998003254

Carson M (1997) Ribbons. In: Sweet RM, Carter CW (eds) Methods in enzymology, vol 277. Academic Press, New York, pp 493–505

CCP4 (1994) The collaborative computational project 4 (CCP4) suite: programs for protein crystallography. Acta Crystallogr D Biol Crystallogr 50:760–763. doi:10.1107/S0907444994003112

Champagne DE, Nussenzweig RH, Ribeiro JMC (1995) Purification, partial characterization, and cloning of nitric oxide-carrying heme proteins (nitrophorins) from salivary glands of the blood-sucking insect *Rhodnius prolixus*. J Biol Chem 15:8691–8695

Chong S-H, Joti Y, Kidera A, Go N, Ostermann A, Gassmann A, Parak FG (2001) Dynamical transition of myoglobin in a crystal: comparative studies of X-ray crystallography and Mössbauer spectroscopy. Eur Biophys J 30:319–329. doi:10.1007/s002490100152

Cooke R, Debrunner P (1968) Mössbauer studies of the iron atom in cytochrome C. J Chem Phys 48:4532–4537. doi:10.1063/1.1668022

Debrunner PG (1989) Mössbauer spectroscopy of iron porphyrins. In: Lever ABP, Gray HB (eds) Iron porphyrins part III, pp 137–234

Ding XD, Weichsel A, Andersen JF, Shokhireva TK, Balfour C, Pierik AJ, Averill BA, Montfort WR, Walker FA (1999) Nitric oxide binding to the ferri- and ferroheme states of nitrophorin 1, a reversible NO-binding heme protein from the saliva of the blood-sucking insect, *Rhodnius prolixus*. J Am Chem Soc 121:128–138. doi:10.1021/ja982979i

Doster W, Settles M (1998) The dynamical transition in proteins: the role of hydrogen bonds. In: Bellissent-Funel M-C (ed) Hydratation processes in biology: theoretical and experimental approaches. IOS Press, Les Houches, pp 177–191

Doster W, Cusack S, Petry W (1989) Dynamical transition of myoglobin revealed by inelastic neutron scattering. Nature 337:754–756. doi:10.1038/337754a0

Drenth J (1998) Principles of protein X-ray crystallography. Springer, Berlin

Engler N, Ostermann A, Gassmann A, Lamb DC, Prusakov VE, Schott J, Schweitzer-Stenner R, Parak FG (2000) Protein dynamics in an intermediate state of myoglobin: optical absorption, resonance Raman spectroscopy, and X-ray structure analysis. Biophys J 78:2081–2092. doi:10.1016/S0006-3495(00)76755-5

Engler N, Ostermann A, Niimura N, Parak FG (2003) Hydrogen atoms in proteins—positions and dynamics. Proc Natl Acad Sci USA 100:10243–10248. doi:10.1073/pnas.1834279100

Fenimore PW, Frauenfelder H, McMahon BH, Parak FG (2002) Slaving: solvent fluctuations dominate protein dynamics and functions. Proc Natl Acad Sci USA 99:16047–16051. doi:10.1073/pnas.212637899

Fenimore PW, Frauenfelder H, McMahon BH, Young RD (2004) Bulk-solvent and hydration-shell fluctuations, similar to α- and β-fluctuations in glasses, control protein motions and functions. Proc Natl Acad Sci USA 101:14408–14413. doi:10.1073/pnas.0405573101

Frauenfelder H, Parak F, Young RD (1988) Conformational substates in proteins. Annu Rev Biophys Biophys Chem 17:451–479. doi:10.1146/annurev.bb.17.060188.002315

Frauenfelder H, Fenimore PW, Chen G, McMahon BH (2006) Protein folding is slaved to solvent motions. Proc Natl Acad Sci USA 103:15469–15472. doi:10.1073/pnas.0607168103

Garbers A, Reifarth F, Kurrek J, Renger G, Parak F (1998) Correlation between protein flexibility and electron transfer from Qa to QB in PSII membrane fragments from spinach. Biochemistry 37:11399–11404. doi:10.1021/bi980296+

Gol'danskii VI, Makarov EF (1968) Fundamentals of gamma-resonance spectroscopy. In: Goldanskii VI, Herber RH (eds) Chemical application of Mössbauer spectroscopy. Academic Press, New York

Hartmann H, Zinser S, Komninos P, Schneider RT, Nienhaus GU, Parak F (1996) X-ray structure determination of a metastable state of carbonmonoxy myoglobin after photodissociation. Proc Natl Acad Sci USA 93:7013–7016. doi:10.1073/pnas.93.14.7013

Hedvig P (1977) Dielectric spectroscopy of polymers. Adam Hilger, Bristol

Huenges A, Achterhold K, Parak FG (2002) Mössbauer spectroscopy in the energy and in the time domain, a crucial tool for the investigation of protein dynamics. Hyperfine Interact 144/145:209–222. doi:10.1023/A:1025405805908

Jones A, Zou JY, Couran SW, Kjeldgaard M (1991) Improved methods for building protein models in electron density maps and the location of errors in these models. Acta Crystallogr A 47:110–119. doi:10.1107/S0108767390010224

Knapp EW, Fischer SF, Parak F (1982) Protein dynamics from Moessbauer spectra. The temperature dependence. J Phys Chem 86:5042–5047. doi:10.1021/j100223a002

Kondrashov DA, Montfort WR (2007) Nonequilibrium dynamics simulations of nitric oxide release: comparative study of nitrophorin and myoglobin. J Phys Chem B 111:9244–9252. doi:10.1021/jp071136n

Kondrashov DA, Roberts SA, Weichsel A, Montfort WR (2004) Protein functional cycle viewed at atomic resolution: conformational change and mobility in nitrophorin 4 as a function of pH and NO binding. Biochemistry 43:13637–13647. doi:10.1021/bi0483155

Lamb DC, Ostermann A, Prusakov VE, Parak FG (1998) From metmyoglobin to deoxy myoglobin: relaxations of an intermediate state. Eur Biophys J 27:113–125. doi:10.1007/s002490050117

Lang G, Herbert D, Yonetani T (1968) Mössbauer spectroscopy of cytochrome C. J Chem Phys 49:944–950. doi:10.1063/1.1670164

Maes EM, Weichsel A, Andersen JF, Shepley D, Montfort WR (2004) Role of binding site loops in controlling nitric oxide release: structure and kinetics of mutant forms of nitrophorin 4. Biochemistry 43:6679–6690. doi:10.1021/bi049748a

Maes EM, Roberts SA, Weichsel A, Montfort WR (2005) Ultrahigh resolution structures of nitrophorin 4: heme distortion in ferrous CO and No complexes. Biochemistry 44:12690–12699. doi:10.1021/bi0506573

Nienhaus K, Maes EM, Weichsel A, Montfort WR (2004) Structural dynamics controls nitric oxide affinity in nitrophorin 4. J Biol Chem 279:39401–39407. doi:10.1074/jbc.M406178200

Ostermann A, Waschipky R, Parak FG, Nienhaus GU (2000) Ligand binding and conformational motions in myoglobin. Nature 404:205–208. doi:10.1038/35004622

Parak FG (2003) Proteins in action: the physics of structural fluctuations and conformational changes. Curr Opin Struct Biol 13:552–557. doi:10.1016/j.sbi.2003.09.004

Parak F, Formanek H (1971) Untersuchung des Schwingungsanteils und des Kristallgitterfehleranteils des Temperaturfaktors in myoglobin durch Vergleich von Mössbauerabsorptionsmessungen mit Röntgenstrukturdaten. Acta Crystallogr A 27:573–578. doi:10.1107/S0567739471001281

Parak F, Frolov EN, Kononenko AA, Mössbauer RL, Goldanskii VI, Rubin AB (1980) Evidence for a correlation between the photoinduced electron transfer and dynamic properties of the chromatophore membranes from *Rhodospirillum rubrum*. FEBS Lett 117:368–372. doi:10.1016/0014-5793(80)80982-3

Parak F, Knapp EW, Kucheida D (1982) Protein dynamics: Mössbauer spectroscopy on deoxymyoglobin crystals. J Mol Biol 161:177–194. doi:10.1016/0022-2836(82)90285-6

Parak F, Fischer M, Graffweg E, Formanek H (1987a) Distributions and fluctuations of protein structures investigated by X-ray analysis and Mössbauer spectroscopy. In: Clementi E, Chin S (eds) Structure and dynamics of nucleic acids, proteins and membranes. pp 139–148

Parak F, Hartmann H, Aumann KD, Reuscher H, Rennekamp G, Bartunik H, Steigemann W (1987b) Low temperatures X-ray investigation of structural distributions in myoglobin. Eur Biophys J 15:237–249. doi:10.1007/BF00577072

Petrova T, Ginell S, Mitschler A, Hazemann I, Schneider T, Cousido A, Lunin VY, Joachimiak A, Podjarny A (2006) Ultrahigh-resolution study of protein atomic displacement parameters at cryotemperatures obtained with a helium cryostat. Acta Crystallogr D Biol Crystallogr 62:1535–1544. doi:10.1107/S0907444906041035

Prusakov VE, Steyer J, Parak FG (1995) Moessbauer spectroscopy on nonequilibrium states of myoglobin: a study of r–t relaxation. Biophys J 68:2524–2530. doi:10.1016/S0006-3495(95)80435-2

Rasmussen BF, Stock AM, Ringe D, Petsko GA (1992) Crystalline ribonuclease A loses function below the dynamical transition at 220 K. Nature 357:423–424. doi:10.1038/357423a0

Ribeiro JMC, Hazzard JMH, Nussenzweig RH, Champagne DE, Walker FA (1993) Reversible binding of nitric oxide by a salivary heme protein from a bloodsucking insect. Science 260:539–541. doi:10.1126/science.8386393

Roberts SA, Weichsel A, Qiu Y, Shelnutt JA, Walker FA, Montfort WR (2001) Ligand-induced heme ruffling and bent NO geometry in ultra-high-resolution structures of nitrophorin 4. Biochemistry 40:11327–11337. doi:10.1021/bi0109257

Schlichting I, Berendzen J, Phillips GN Jr, Sweet RM (1994) Crystal structure of photolysed carbonmonoxy-myoglobin. Nature 371:808–812. doi:10.1038/371808a0

Sharrock M, Münck E, Debrunner PG, Marshall V, Lipscomb JD, Gunsalus IC (1973) Mössbauer studies of cytochrome P-450$_{cam}$. Biochemistry 12:258–265. doi:10.1021/bi00726a013

Shibata Y, Kurita A, Kushida T (1998) Real-time observation of conformational fluctuations in Zn-substituted myoglobin by time-resolved transient hole-burning spectroscopy. Biophys J 75:521–527. doi:10.1016/S0006-3495(98)77541-1

Singh GP, Parak F, Hunklinger S, Dransfeld K (1981) Role of adsorbed water in the dynamics of metmyoglobin. Phys Rev Lett 47:685–688. doi:10.1103/PhysRevLett.47.685

Steinbach PJ, Ansari A, Berendzen J, Braunstein D, Chu K, Cowen BR, Ehrenstein D, Frauenfelder H, Johnson JB, Lamb DC, Mourant JR, GUl Nienhaus, Ormos P, Philipp R, Xie A, Young RD (1991) Ligand binding to heme proteins: connection between dynamics and function. Biochemistry 30:3988–4001. doi:10.1021/bi00230a026

Teng T-Y, Šrajer V, Moffat K (1994) Photolysis-induced structural changes in single crystals of carbonmonoxy myoglobin at 40 K. Struct Biol 1:701–705. doi:10.1038/nsb1094-701

Teng T-Y, Šrajer V, Moffat K (1997) Initial trajectory of carbon monoxide after photodissociation from myoglobin at cryogenic temperatures. Biochemistry 36:12087–12100. doi:10.1021/bi971140x

Walker FA (2005) Nitric oxide interaction with insect nitrophorins and thoughts on the electron configuration of the {FeNO}^{6} complex. J Inorg Biochem 99:216–236. doi:10.1016/j.jinorgbio.2004.10.009

Walker FA, Montfort wR (2000) The nitric oxide-releasing heme proteins from the saliva of the blood-sucking insect *Rhodnius prolixus*. Adv Inorg Chem 51:295–358. doi:10.1016/S0898-8838(00)51006-X

Weichsel A, Andersen JF, Champagne DE, Walker FA, Montfort WR (1998) Crystal structures of a nitric oxide transport protein from a blood-sucking insect. Nat Struct Biol 5:304–309. doi:10.1038/nsb0498-304